Supporting Information

Three-dimensional N-doped carbon nanosheets loading heterostructured Ni/Ni$_3$ZnC$_{0.7}$ nanoparticles for Selective and Efficient CO$_2$ Reduction

Li Liao[a, 1], Chunguang Jia[a, 1], Songjiang Wu[a], Shenjie Yu[a], Zhenhai Wen[a,b,*], Suqin Ci[a,*]

[a] *Key Laboratory of Jiangxi Province for Persistent Pollutants Control, National-Local Joint Engineering Research Center of Heavy Metals Pollutants Control and Resource Utilization and Resources Recycle, Nanchang Hangkong University, Nanchang, 330063, Jiangxi, China*

[b] *CAS Key Laboratory of Design and Assembly of Functional Nanostructures, and Fujian Provincial Key Laboratory of Materials and Techniques toward Hydrogen Energy, Fujian Institute of Research on the Structure of Matter, Chinese Academy of Sciences, Fuzhou, Fujian, 350002, China*

[1]: These authors contributed equally to this -work.

* Corresponding authors.

E-mail: sqci@nchu.edu.cn, wen@fjirsm.ac.cn

Experimental Part

1. Chemicals

All reagents and chemicals were obtained commercially and used without any further purification. The sources of these chemicals were as follows: Trisodium citrate dihydrate ($Na_3C_6H_5O_7 \cdot 2H_2O$, 99%), Nickel nitrate hexahydrate ($Ni(NO_3)_2 \cdot 6H_2O$, 98%), Zinc nitrate hexahydrate ($Zn(NO_3)_2 \cdot 6H_2O$, 99%) and Ethanol (C_2H_5OH, 95%) were purchased from Xilong Chemical Co., Ltd., D-Glucosamine hydrochloride ($C_6H_{14}ClNO_5$, 98%), Sodium Hydroxide (NaOH, 98%) and Potassium chloride (KCl, 99%) from Adamas, N-Cyanoguanidin ($C_2H_4N_4$, 99%) from Macklin, Potassium Bicarbonate ($KHCO_3$, 99%), Potassium Hydroxide (KOH, 90%) and H_2SO_4 (98%) from Greagent, and Nafion perfluorinated resin ($C_9HF_{17}O_5S$, 5 wt%) from Alfa.

2. Characterization

Scanning electron microscope (SEM) images were showed by SU-8010 (ZEISS) at an acceleration voltage of 10 kV. Field emission transmission electron microscopy (TEM) and the corresponding energy dispersion spectral mapping (EDS) were performed on FEI TF20 and Super-X at an acceleration voltage of 200 kV, respectively. The X-ray powder diffraction pattern was obtained by D8ADVANCE-A25 X-ray diffractometer. The chemical structure of the catalyst was explored using X-ray photoelectron spectroscopy (XPS, Thermo Scientific K-Alpha, Al Ka). The raw data were calibrated from a C 1s peak of 284.8 eV. Raman spectra were measured by LabRAM HR. The specific surface area and pore structure of all catalysts were analyzed by specific surface and pore size distribution analyzer (Quantachrome NovaWin).
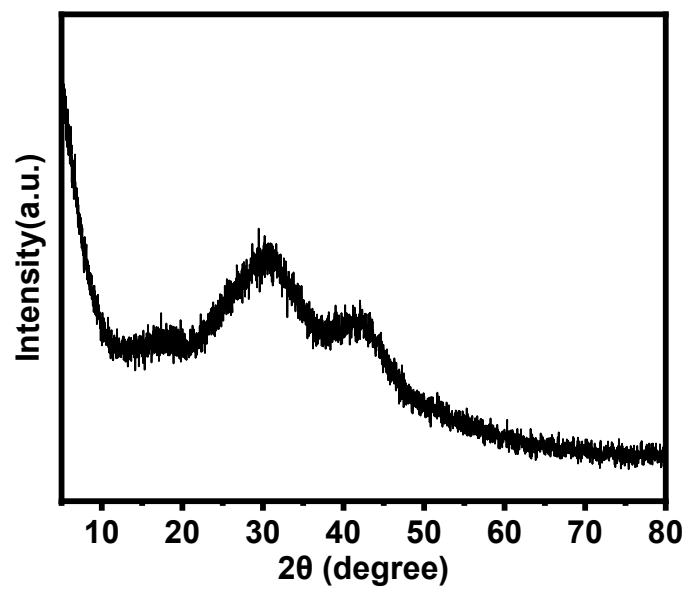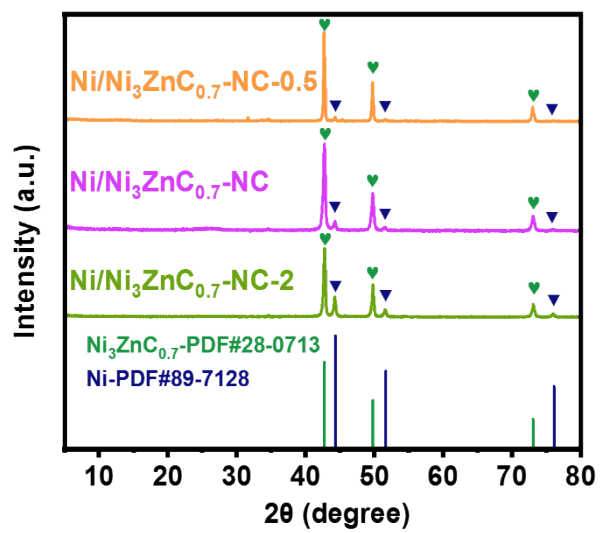
Fig. S1. XRD of carbon nanosheet.

Fig. S2. XRD patterns of Ni/Ni$_3$ZnC$_{0.7}$-NC-0.5, Ni/Ni$_3$ZnC$_{0.7}$-NC and Ni/Ni$_3$ZnC$_{0.7}$-NC-2 catalysts.
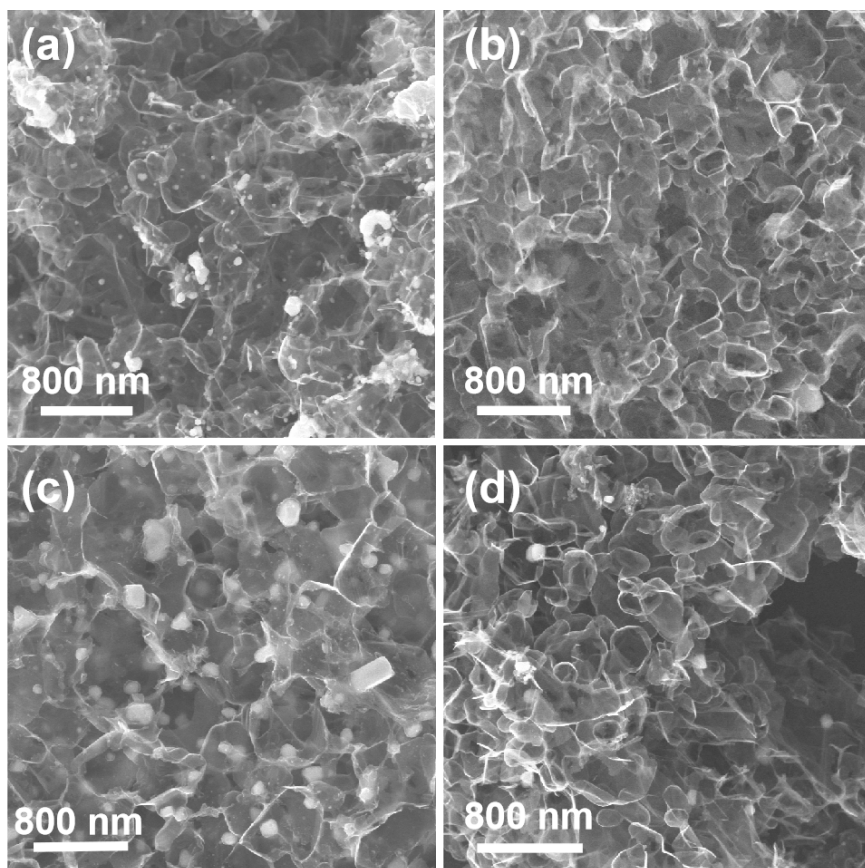
Fig. S3. SEM images of the (a) $Ni_3ZnC_{0.7}$-NC, (b) Ni-NC, (c) $Ni/Ni_3ZnC_{0.7}$-NC-0.5 and (d) $Ni/Ni_3ZnC_{0.7}$-NC-2 catalysts.
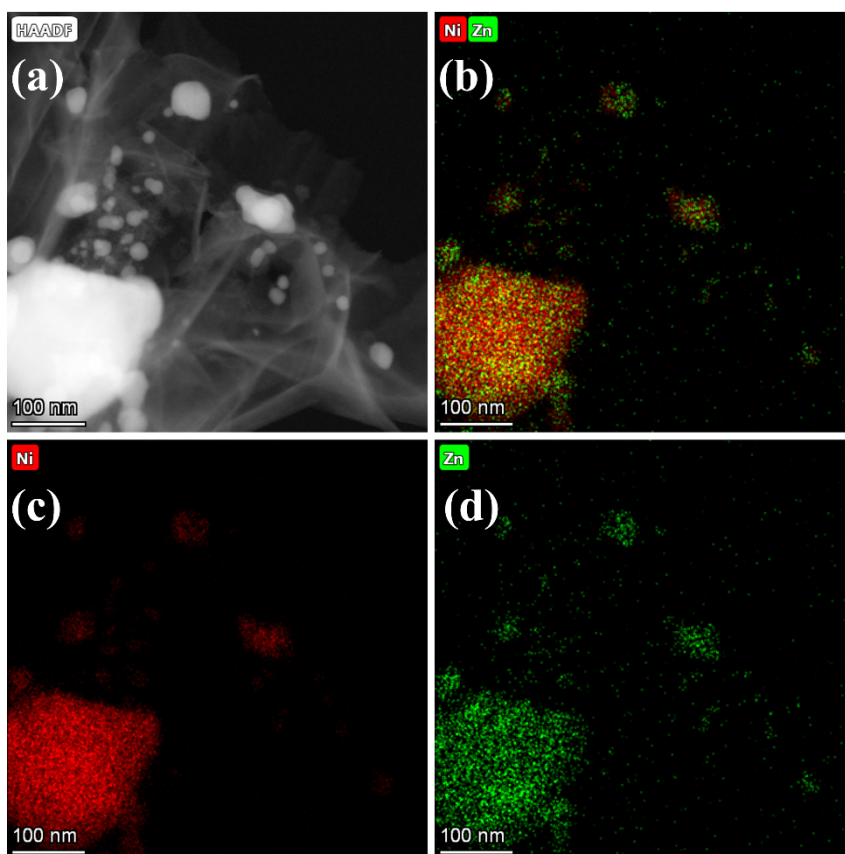
Fig. S4. (a) STEM image of Ni/Ni$_3$ZnC$_{0.7}$-NC (metal nanoparticle spheres) (b),(c),(d)the corresponding elemental mapping of Ni and Zn.
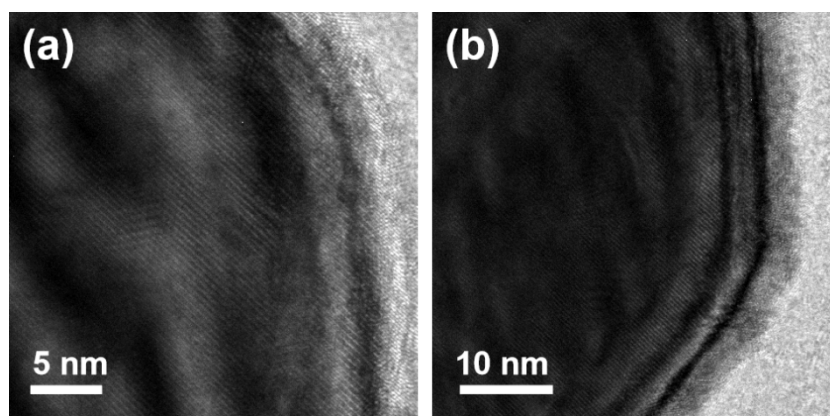
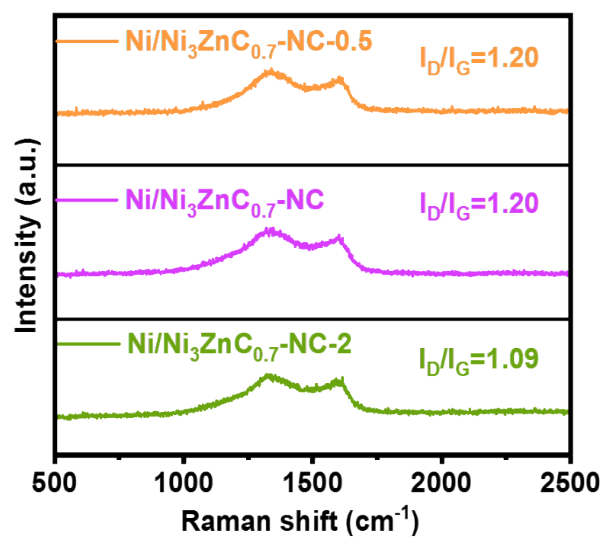**Fig. S5.** (a) and (b) HRTEM images of the Ni/Ni$_3$ZnC$_{0.7}$-NC.

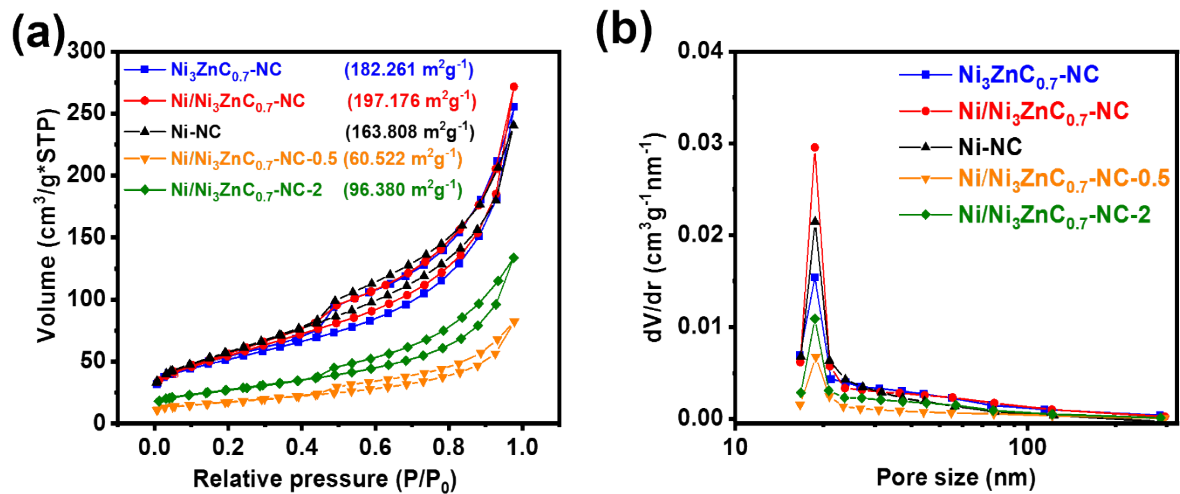**Fig. S6.** Raman spectra of $Ni/Ni_3ZnC_{0.7}$-NC-0.5, $Ni/Ni_3ZnC_{0.7}$-NC and $Ni/Ni_3ZnC_{0.7}$-NC-2.

Fig. S7. (a) N_2 adsorption-desorption isotherms, (b) Pore size distribution of $Ni_3ZnC_{0.7}$-NC, $Ni/Ni_3ZnC_{0.7}$-NC, Ni-NC, $Ni/Ni_3ZnC_{0.7}$-NC-0.5 and $Ni/Ni_3ZnC_{0.7}$-NC-2.
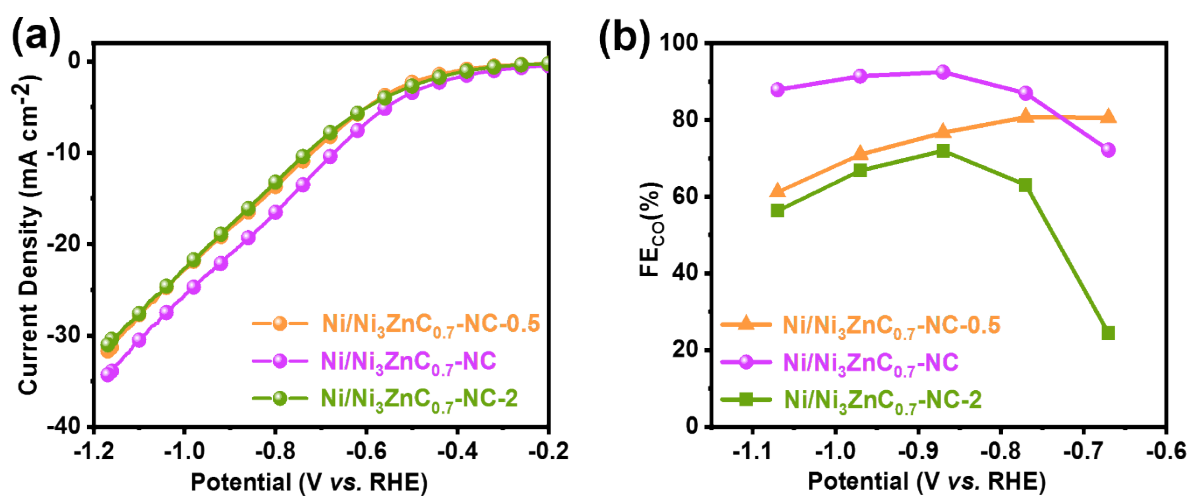
Fig. S8. Ni/Ni$_3$ZnC$_{0.7}$-NC-0.5, Ni/Ni$_3$ZnC$_{0.7}$-NC and Ni/Ni$_3$ZnC$_{0.7}$-NC-2 of: (a) LSV curves, (b) FE$_{CO}$.
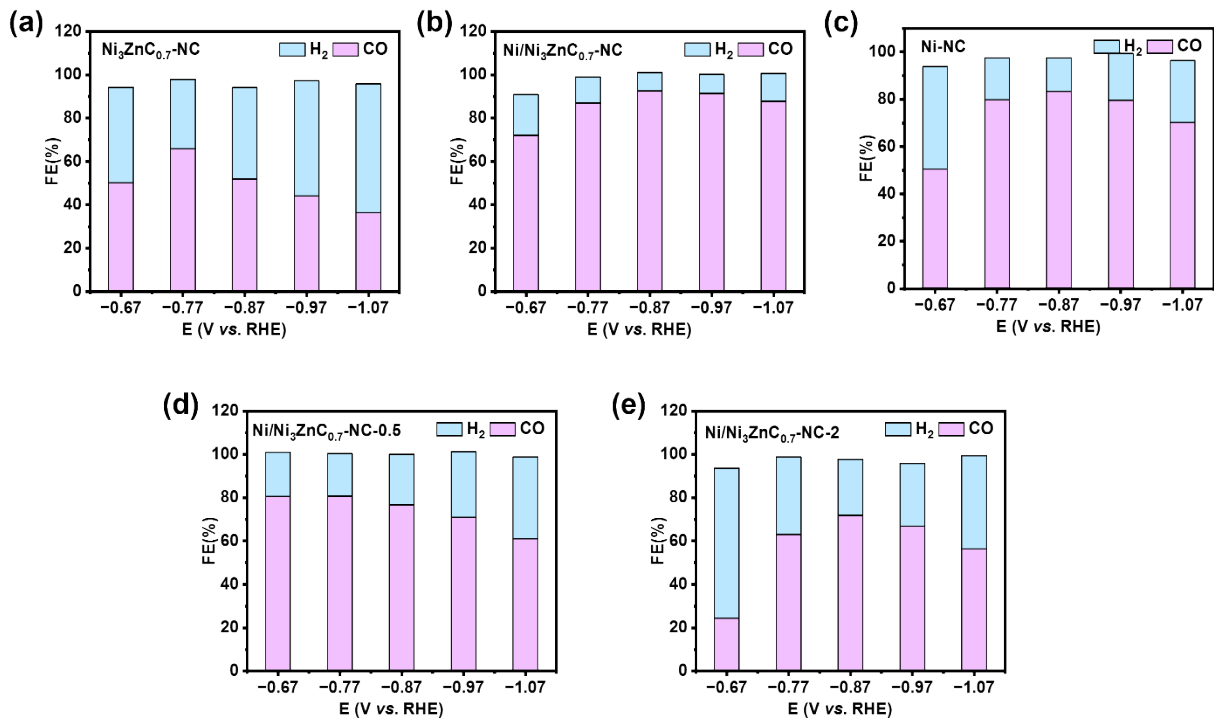
Fig. S9. The total FE of (a) $Ni_3ZnC_{0.7}$-NC, (b) $Ni/Ni_3ZnC_{0.7}$-NC, (c) Ni-NC, (d) $Ni/Ni_3ZnC_{0.7}$-NC-0.5, (e) $Ni/Ni_3ZnC_{0.7}$-NC-2.
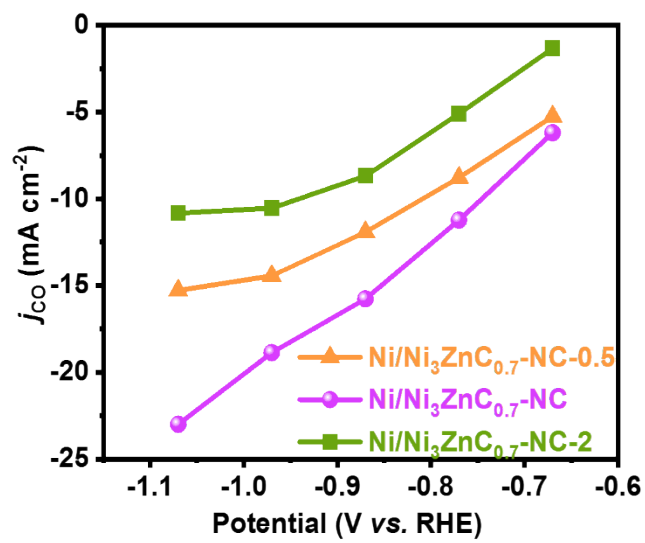
Fig. S10. j_{CO} of Ni/Ni$_3$ZnC$_{0.7}$-NC-0.5, Ni/Ni$_3$ZnC$_{0.7}$-NC and Ni/Ni$_3$ZnC$_{0.7}$-NC-2.
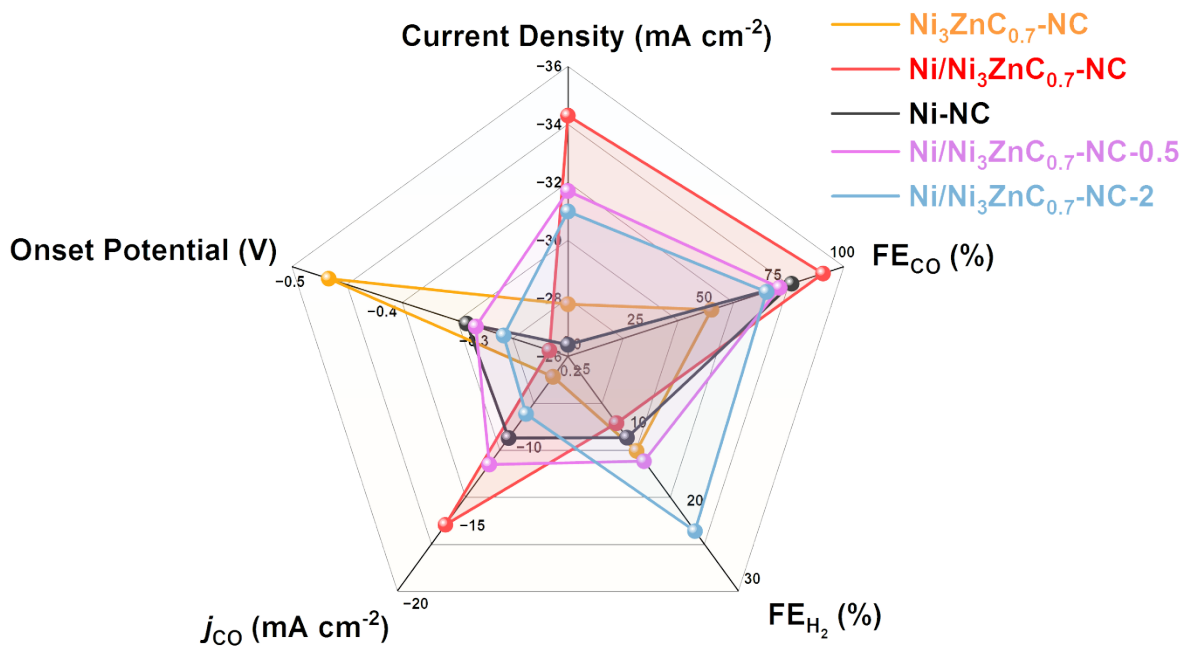
Fig. S11. Comparison of current density at -1.17 V *vs.* RHE, FE_{CO}, FE_{H_2} and j_{CO} at -0.87 V *vs.* RHE, and onset potential at 1 mA cm^{-2} of Ni$_3$ZnC$_{0.7}$-NC, Ni/Ni$_3$ZnC$_{0.7}$-NC, Ni-NC, Ni/Ni$_3$ZnC$_{0.7}$-NC-0.5 and Ni/Ni$_3$ZnC$_{0.7}$-NC-2.
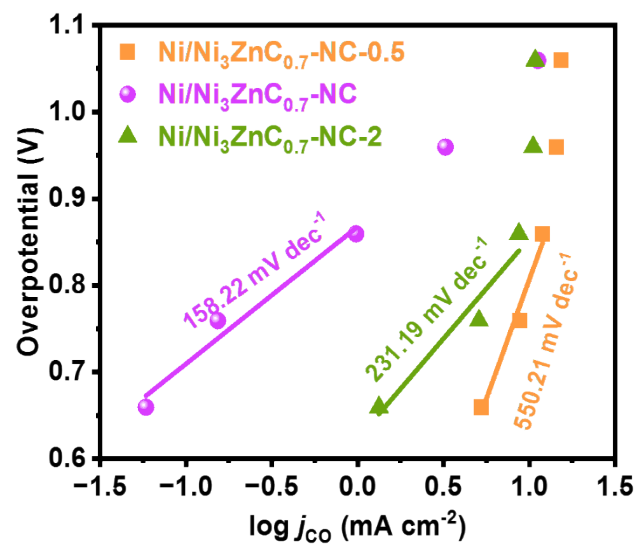
Fig. S12. Tafel plots of Ni/Ni$_3$ZnC$_{0.7}$-NC-0.5, Ni/Ni$_3$ZnC$_{0.7}$-NC and Ni/Ni$_3$ZnC$_{0.7}$-NC-2.
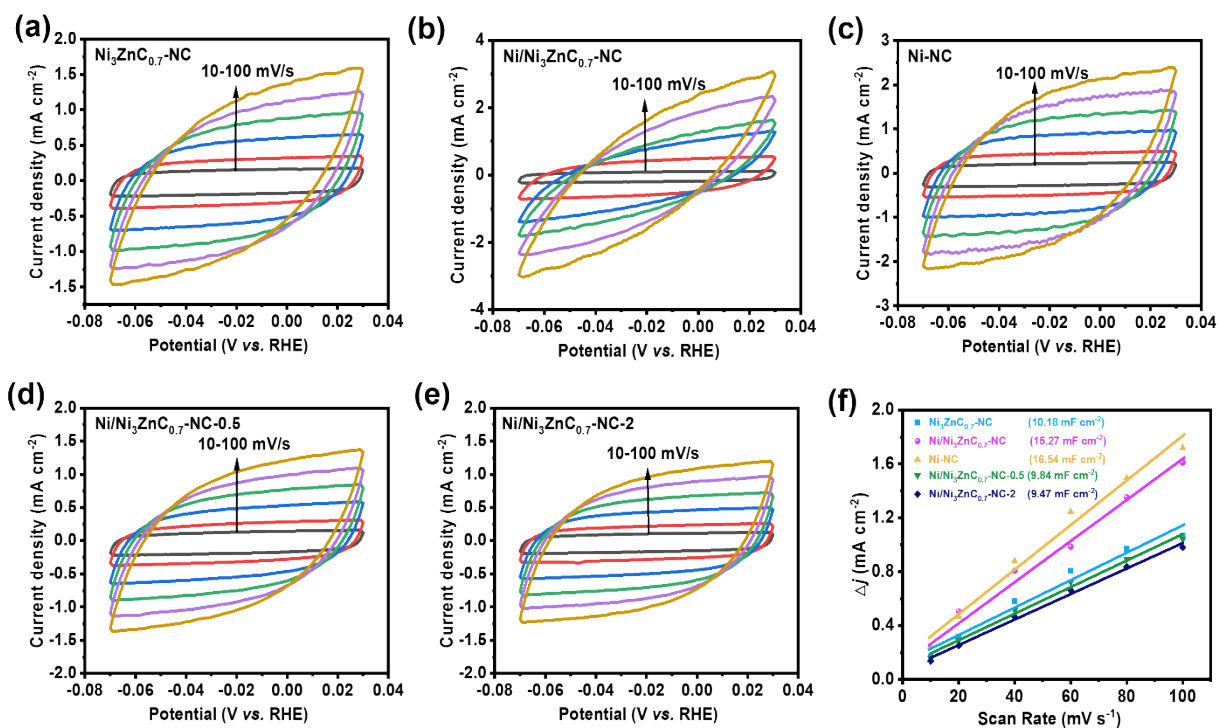
Fig. S13. Cyclic voltammograms of (a) $Ni_3ZnC_{0.7}$-NC, (b) $Ni/Ni_3ZnC_{0.7}$-NC, (c) Ni-NC, (d) $Ni/Ni_3ZnC_{0.7}$-NC-0.5, (e) $Ni/Ni_3ZnC_{0.7}$-NC-2 catalysts recorded between -0.03-0.07 V *vs.* RHE at the different sweep rate in CO_2-saturated 0.5 M $KHCO_3$ electrolyte, (f) Plot of double layer current densities obtained at -0.02 V *vs.* RHE.
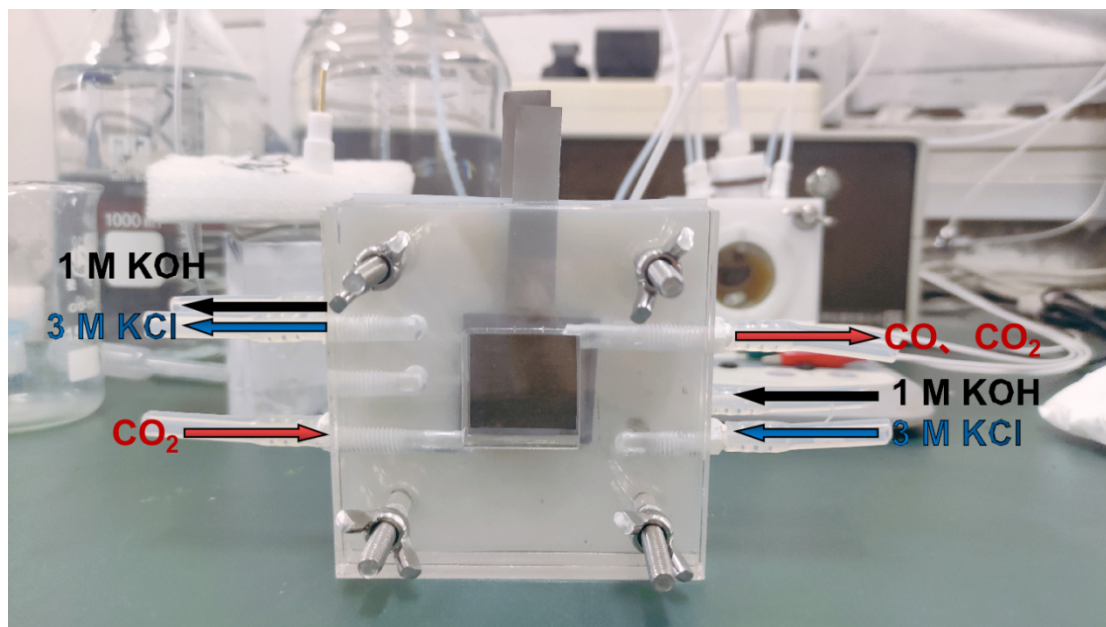
Fig. S14. Physical drawing of flow cell.

Fig. S15. The Pourbaix diagram of water with curves generated by the Nernst equation showing the theoretical potentials for the corresponding reactions.

Fig. S16. Formation of carbonate precipitate on the carbon paper after the reaction.

DFT calculations details

1. DFT parameters

All the calculations are implemented by PWSCF codes contained in the Quantum ESPRESSO distribution [1]. Spin-polarized DFT calculations were performed with periodic super-cells under the generalized gradient approximation (GGA) using the Perdew-Burke-Ernzerhof (PBE) func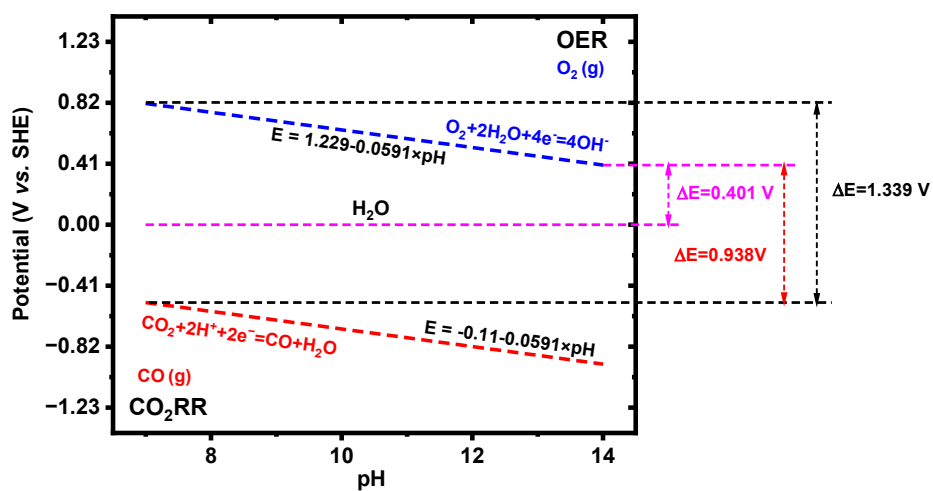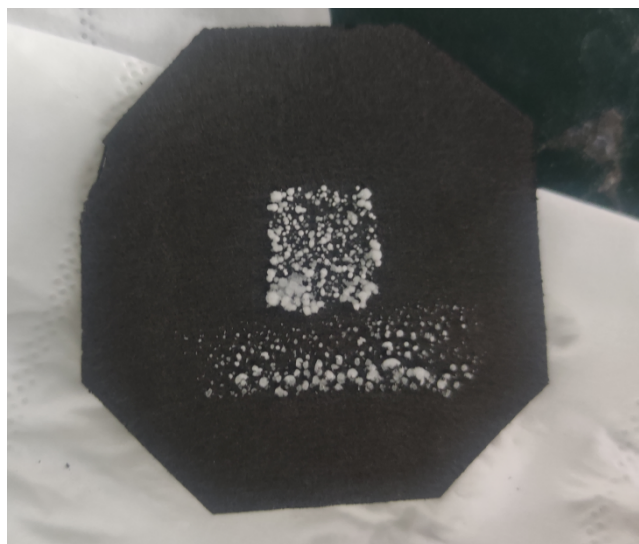tional for exchange-correlation and the ultrasoft pseudopotentials for nuclei and core electrons. The Kohn-Sham orbitals were expanded in a plane-wave basis set with a kinetic energy cutoff of 30 Ry and the charge-density cutoff of 300 Ry. The Fermi-surface effects has been treated by the smearing technique of Methfessel and Paxton, using a smearing parameter of 0.02 Ry. Periodical supercells containing single-layer graphene with 15 Å vacuum above were used to model various graphene doping structures. To model the doping N in the basal plane, we used the super cell of lateral size 4×4. For the doping N in the edge, we used the super cell of lateral size 3×5. For $Ni_3ZnC_{0.7}$ (001) 2×2 supercell and two-layer slab are utilized. The bottom one-layer is fixed to model $Ni_3ZnC_{0.7}$ bulk. For Ni (001) 2×2 supercell and four-layer slab are utilized. The bottom two-layer is fixed to model Ni bulk. The Brillouin zone was sampled with (1×1×1) Monkhorst-Pack k-points.

2. A brief introduction of the computational hydrogen electrode (CHE) method.

Generally speaking, when studying about the electrocatalytic reaction through first principle, there are two difficulties, one is to calculate the reaction barrier of the proton coupled electron transfer (PCET) reaction, the other is the Gibbs free energy of the solvated H^+. The CHE method [2] proposed by Norskov et al is aiming at settling or bypassing these two difficulties. In the framework of CHE method, for the reaction

$$H^+ + e^- \rightarrow \frac{1}{2}H_2$$

(S1)

reaches equilibrium on $U_{SHE}=0$ V, one can replace the energy of H^+ with that of $1/2H_2$:

$$G_{H^+} = \frac{1}{2}G_{H_2}$$

(S2)

The energy of electron can be expressed by $–Ue$, where U is the electrode potential *vs*. SHE. As for the reaction barrier of PCET, the CHE method assumes the overpotential of the electrocatalytic reaction is the overpotential least to make standard reaction Gibbs free energies of

all the elementary step to be exothermic. And such potential is called the reaction limiting potential, which is denoted as U_l. Usually, U_l is an activity descriptor, as for CO_2RR, U_l can be used to judge the exact reaction pathway.

3. The reaction models and pathway

The reaction mechanisms for CO_2RR written as follows:

$$CO_2 + H^+ + e^- + * \rightarrow COOH^* \tag{S3}$$

$$COOH^* + H^+ + e^- \rightarrow CO^* + H_2O(l) \tag{S4}$$

$$CO^* \rightarrow CO(g) + * \tag{S5}$$
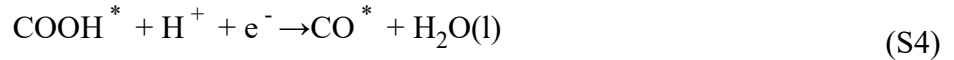
The asterisk stands for the sites on the surface of the catalysts.

In calculating the Gibbs free energy differences from R1 to R5, the associated adsorption free energy of the adsorbates is calculated by the following expression:

$$G_A = ZPE - TS + \int C_p dT \tag{S6}$$

Where E_A is the total energy of a certain molecule or adsorbate A*. When A is representing a certain molecule, the total energies can be calculated directly. When A is representing a certain adsorbate, it is calculated by the difference between the DFT based substrate with (E_{A*}^{DFT}) and without adsorbate A (E_*^{DFT}):

$$E_A = E_{A^*}^{DFT} - E_*^{DFT} \tag{S7}$$

ZPE, TS and $\int C_p dT$ are the correction from zero point energy, entropy and heat capacity, whose values are listed on Table S1. Other than that, H^+ is calculated by the Gibbs free energy of $1/2H_2$, the energy of electron is calculated by $-Ue$. A correction of -0.51 eV is added to CO molecules for the errors for GGA-PBE functional. According to Ref. [3] such correction can lead an agreement with experimental overall half reaction of CO_2 reduction.
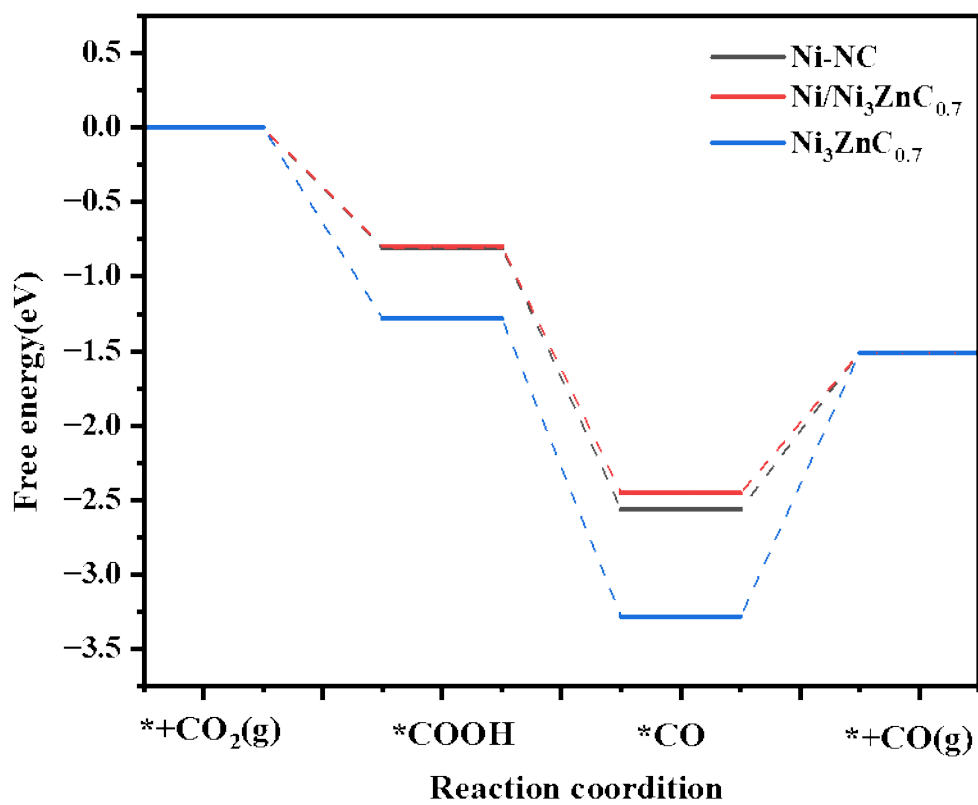
Fig.S17. The free energy diagrams (FED) of CO_2RR reacts on Ni-NC, $Ni/Ni_3ZnC_{0.7}$ and $Ni_3ZnC_{0.7}$

top

left

O
H
C
Zn
Ni

blank   *COOH   *CO
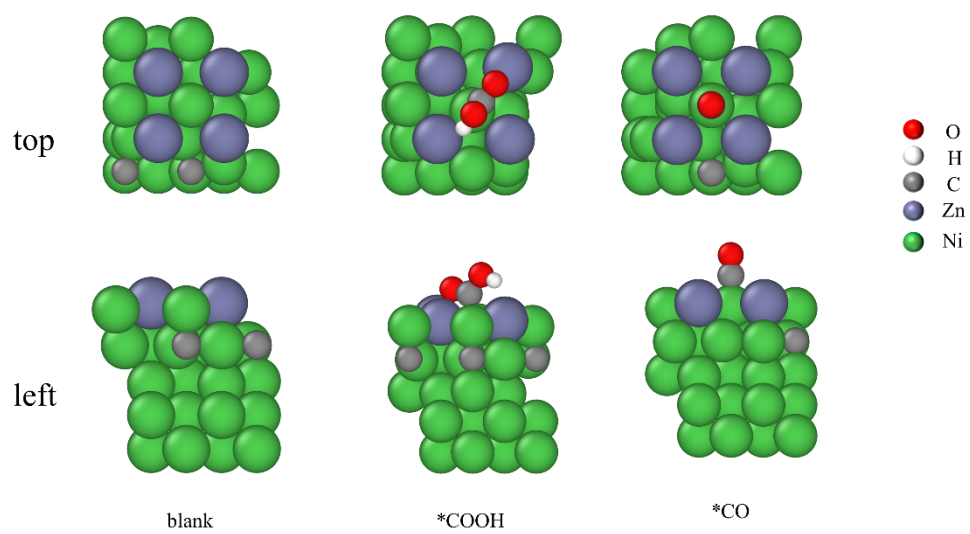
Fig.S18. Stable configures of Ni/Ni$_3$ZnC$_{0.7}$
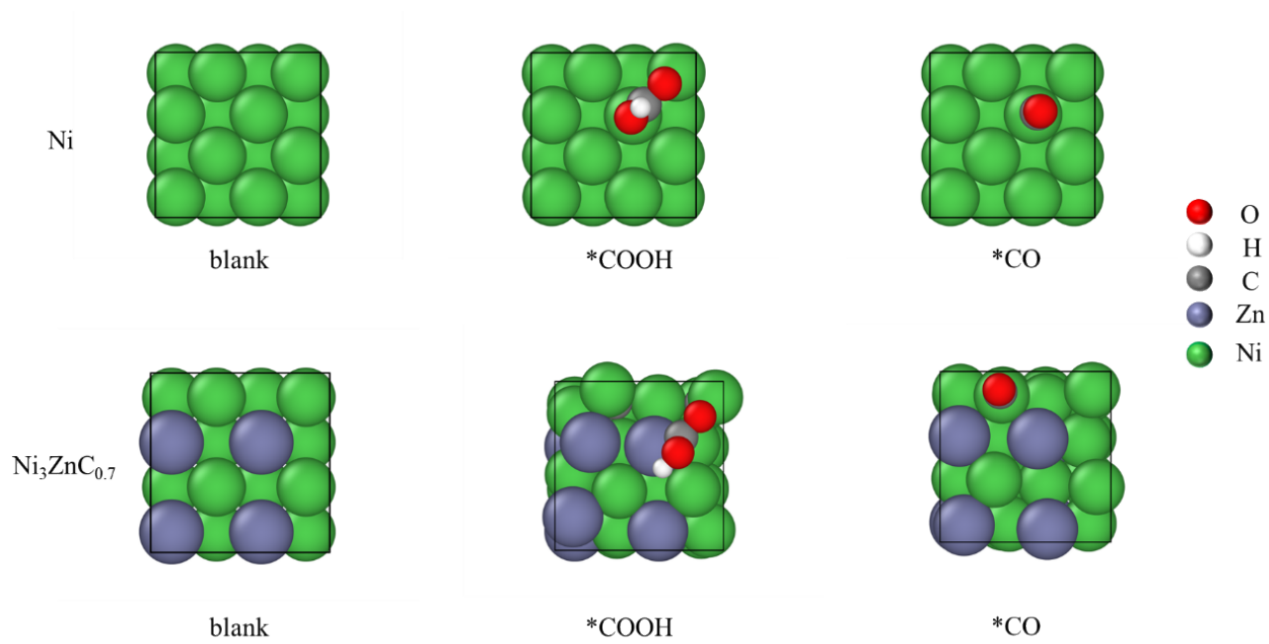
Fig. S19. Stable configures of Ni and $Ni_3ZnC_{0.7}$.
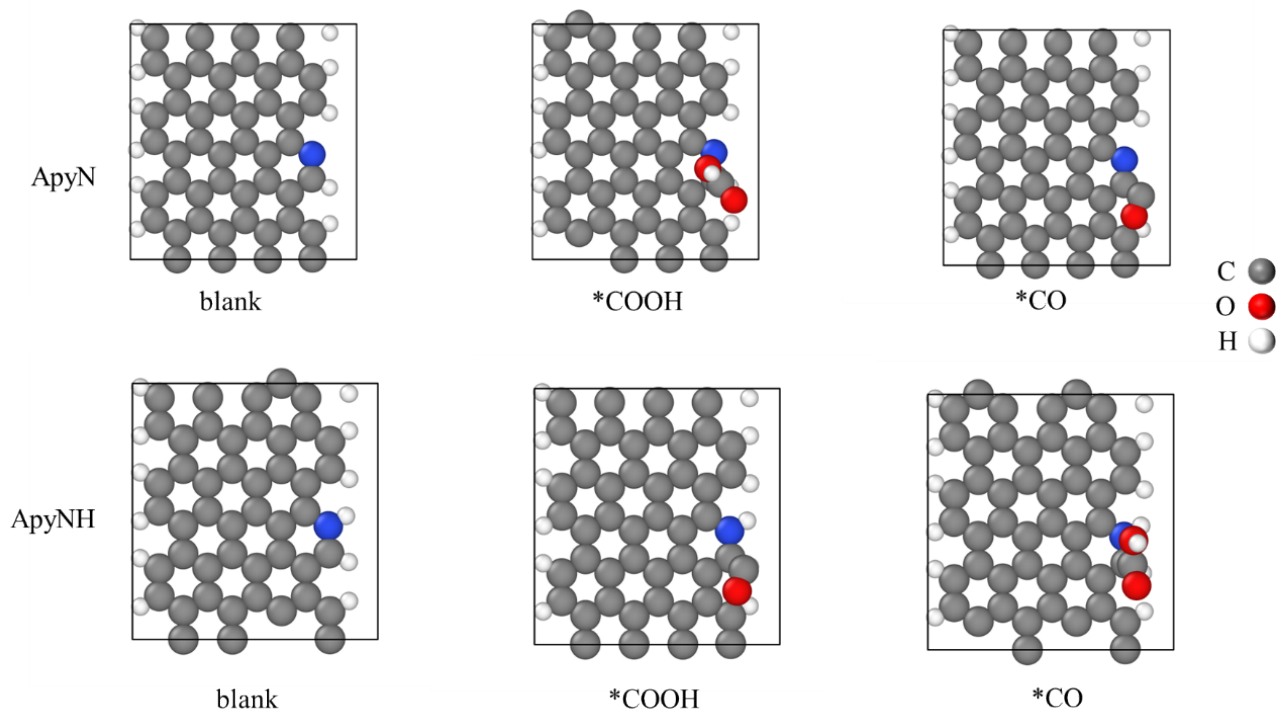
Fig. S20. Stable configures of pyridinic N at edge with and without hydrogeneration (ApyN and ApyNH).
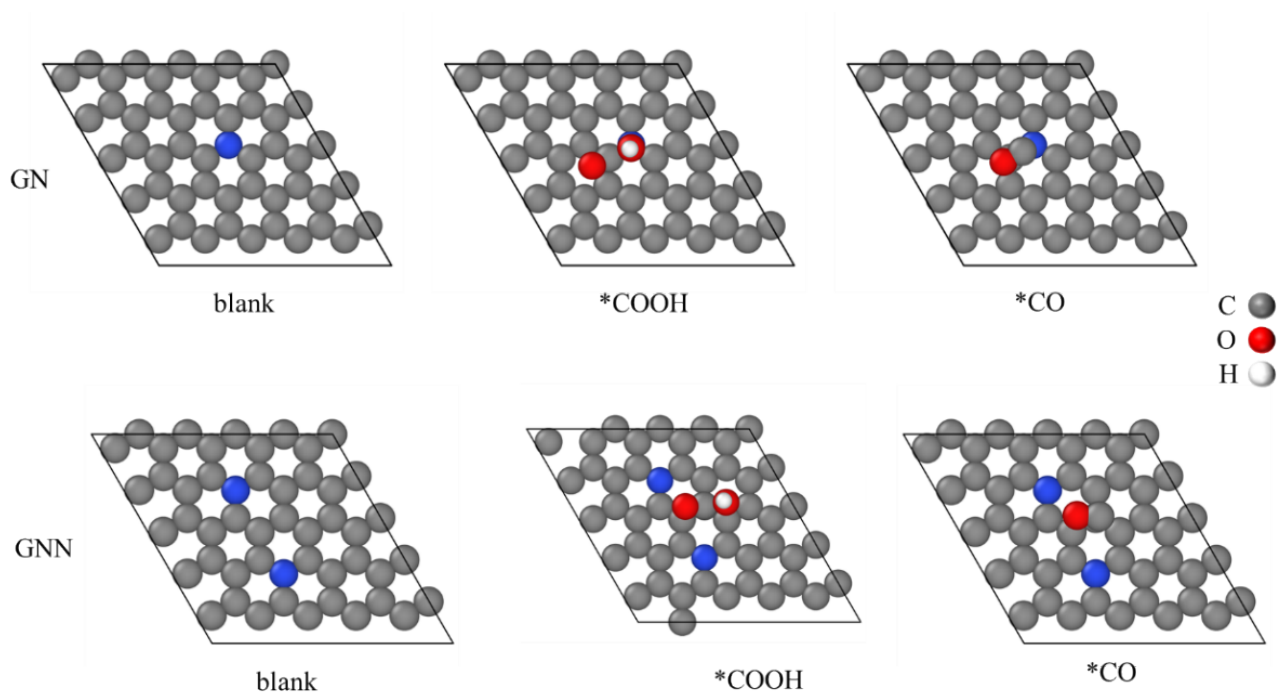
Fig. S21. Stable configures of N doped graphene (GN) and dual N doped graphene (GNN).

pyrroleNH

blank   *COOH   *CO
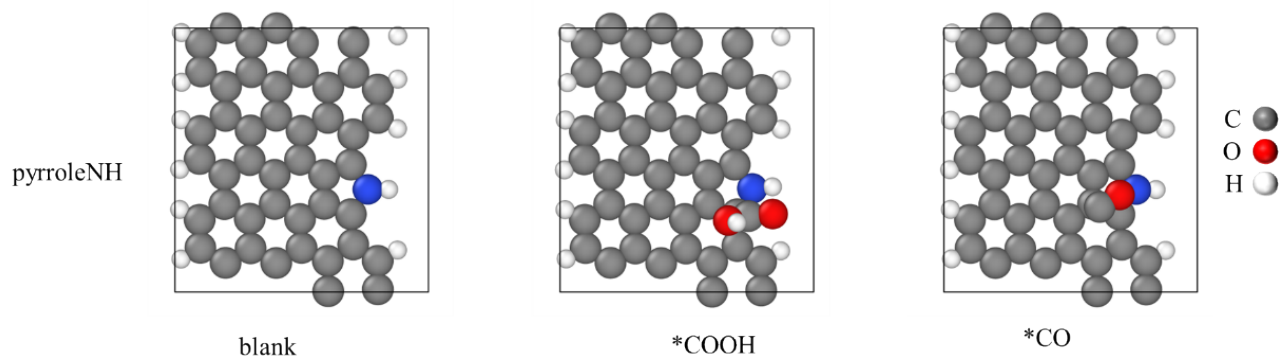
Fig. S22. Stable configures of N doped pyrrole edge (pyrroleNH).
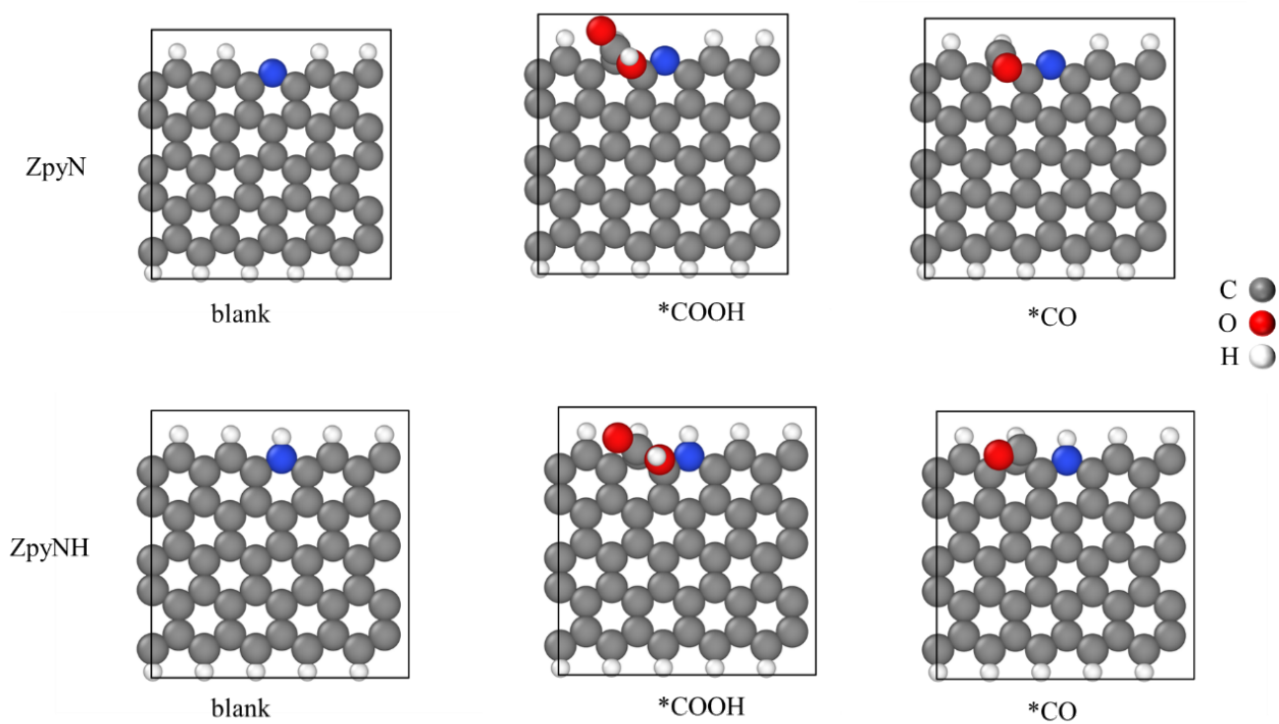
Fig. S23. Stable configures of the zigzag edge sites with and without hydrogeneration (ZpyN and ZpyNH).
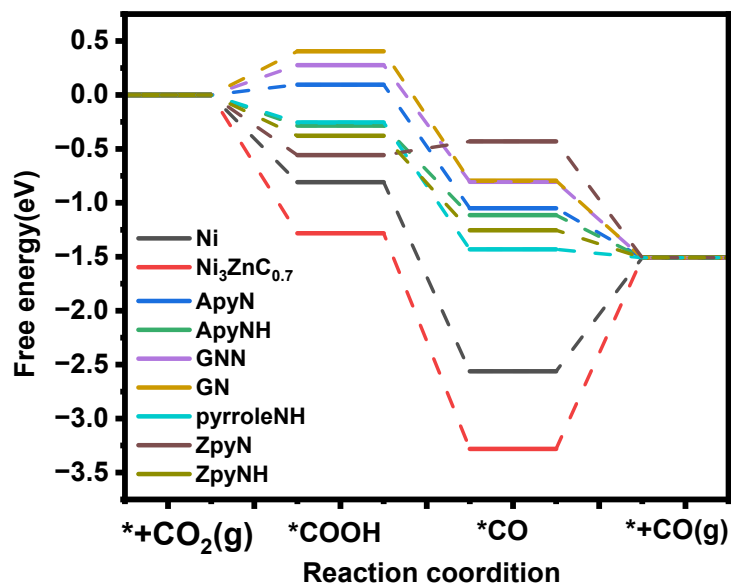
Fig. S24. The free energy diagrams (FED) of CO₂RR.

Table S1. Correction for converting the total energy to Gibbs free energy (in eV) from zero-point energy, entropy and heat capacity. All relevant values are taken from these references [4-8].

Species	ZPE	TS	$\int C_p dT$
COOH*	0.41	0.17	0.09
CO*	0.11	0.08	0.05
H_2	0.27	0.42	0.09
H_2O	0.58	0.42	0.09

Table S2. Summaries of characterization parameters (such as specific surface area, pore volume and ECSA) for $Ni_3ZnC_{0.7}$-NC, $Ni/Ni_3ZnC_{0.7}$-NC, Ni-NC, $Ni/Ni_3ZnC_{0.7}$-NC-0.5 and $Ni/Ni_3ZnC_{0.7}$-NC-2 samples.

Samples	S_{BET} (m^2 g^{-1})	Pore volume (cm^3 g^{-1})	ECSA (mF cm^{-2})
$Ni_3ZnC_{0.7}$-NC	182.261	0.376	10.18
$Ni/Ni_3ZnC_{0.7}$-NC	197.176	0.381	15.27
Ni-NC	163.808	0.335	16.34
$Ni/Ni_3ZnC_{0.7}$-NC-0.5	60.522	0.119	9.84
$Ni/Ni_3ZnC_{0.7}$-NC-2	96.380	0.199	9.47

Table S3. A summary of the reported Ni-based CO_2RR electrocatalysts.

Catalyst	Potential (V *vs*. RHE)	FE_{CO} (%)	j_{CO} (mA cm^{-2})	References
Ni/Ni$_3$ZnC$_{0.7}$-NC	-0.87	92.47	15.77	This work
Ni/Ni$_3$ZnC$_{0.7}$-0.4	-1.0	91.5	11	[9]
Ni$_4$N/Ni$_3$ZnC$_{0.7}$	-0.8	92.3	14.6	[10]
Ni SAs/N-C	-0.89	71.9	7.4	[11]
Ni SAs	-0.8	91	6	[12]
Ni-N-C	-0.85	80	12	[13]
NiOx/FePc	-0.7	60	11.6	[13]
NiN-GS	-0.82	93.2	4	[14]

Table S4. A comparison of previously reported Zn-CO_2 batteries with the Zn//Ni/Ni$_3$ZnC$_{0.7}$-NC battery in this study.

Anode//cathode	Anode electrolyte	Cathode electrolyte	Power density (mW cm^{-2})	Ref.
Zn//Ni/Ni$_3$ZnC$_{0.7}$-NC	4 M NaOH	0.5 M KHCO$_3$	4.2	This work
Zn//Ni$_4$N/Ni$_3$ZnC$_{0.7}$	6 M KOH and 0.2 M Zn(CH$_3$COO)$_2$	0.1 M KHCO$_3$	0.85	[10]
Zn//FeN$_4$Cl/NC-7.5	0.8 M KOH and 0.02 M Zn(CH$_3$COO)$_2$	0.8 M KHCO$_3$	0.545	[15]
Zn//NOMC	6 M KOH and 0.2 M Zn(CH$_3$COO)$_2$	0.8 M KHCO$_3$	0.71	[16]
Zn//Cu-N$_2$/GN	6 M KOH and 0.2 M Zn(CH$_3$COO)$_2$	0.1 M KHCO$_3$	0.6	[17]

Reference

[1] P. Giannozzi, S. Baroni, N. Bonini, M. Calandra, R. Car, C. Cavazzoni, D. Ceresoli, G. L. Chiarotti, M. Cococcioni, I. Dabo, A. Dal Corso, S. de Gironcoli, S. Fabris, G. Fratesi, R. Gebauer, U. Gerstmann, C. Gougoussis, A. Kokalj, M. Lazzeri, L. Martin-Samos, N. Marzari, F. Mauri, R. Mazzarello, S. Paolini, A. Pasquarello, L. Paulatto, C. Sbraccia, S. Scandolo, G. Sclauzero, A. P. Seitsonen, A. Smogunov, P. Umari and R. M. Wentzcovitch, *J. Phys. Condens. Mat.*, 2009, **21**, 395502.

[2] J. K. Nørskov, J. Rossmeisl, A. Logadottir, L. Lindqvist, J. R. Kitchin, T. Bligaard and H. Jónsson, *Phys. Chem. B*, 2004, **108(46)**, 17886–17892.

[3] G. Chai, C. Lin, J. Wang, M. Zhang, J. Wei and W. Cheng, *J. Phys. Chem. C*, 2011, **115**, 2907-2913.

[4] L. C. Grabow and M. Mavrikakis, *ACS Catal.*, 2011, **1**, 365-384.

[5] H. A. Hansen, J. B. Varley, A. A. Peterson and J. K. Norskov, *J. Phys. Chem. Lett.*, 2013, **4**, 388-392.

[6] P. Hirunsit, *J. Phys. Chem. C*, 2013, **117**, 8262-8268.

[7] M. Karamad, H. A. Hansen, J. Rossmeisl and J. K. Nørskov, *ACS Catal.*, 2015, **5**, 4075-4081.

[8] M. Liu, Y. Pang, B. Zhang, P. De Luna, O. Voznyy, J. Xu, X. Zheng, C. T. Dinh, F. Fan, C. Cao, F. P. de Arquer, T. S. Safaei, A. Mepham, A. Klinkova, E. Kumacheva, T. Filleter, D. Sinton, S. O. Kelley and E. H. Sargent, *Nature*, 2016, **537**, 382-386.

[9] X. Wei, S. Xiao, R. Wu, Z. Zhu, L. Zhao, Z. Li, J. Wang, J. S. Chen and Z. Wei, *Appl. Catal. B*, 2022, **302**, 120861.

[10] J. Wang, Z. Li, Z. Zhu, J. Jiang, Y. Li, J. Chen, X. Niu, J. S. Chen and R. Wu, *J. Energy Chem.*, 2022, **75**, 1-7.

[11] C. Zhao, X. Dai, T. Yao, W. Chen, X. Wang, J. Wang, J. Yang, S. Wei, Y. Wu and Y. Li, *J. Am. Chem. Soc.*, 2017, **139**, 8078-8081.

[12] M. Zhang, T.-S. Wu, S. Hong, Q. Fan, Y.-L. Soo, J. Masa, J. Qiu and Z. Sun, *ACS Sustain. Chem. Eng.*, 2019, **7**, 15030-15035.

[13] Y. Cheng, J.-P. Veder, L. Thomsen, S. Zhao, M. Saunders, R. Demichelis, C. Liu, R. De Marco and S. P. Jiang, *J. Mater. Chem. A*, 2018, **6**, 1370-1375.

[14] K. Jiang, S. Siahrostami, A. J. Akey, Y. Li, Z. Lu, J. Lattimer, Y. Hu, C. Stokes, M. Gangishetty, G. Chen, Y. Zhou, W. Hill, W.-B. Cai, D. Bell, K. Chan, J. K. Nørskov, Y. Cui and H. Wang, *Chem.*, 2017, **3**, 950-960.

[15]. S. Ye, G. Fan, J. Xu, L. Yang and F. Li, *Electrochim. Acta*, 2020, **334**, 135583.

[16] S. Gao, Y. Liu, Z. Xie, Y. Qiu, L. Zhuo, Y. Qin, J. Ren, S. Zhang, G. Hu, J. Luo and X. Liu, *Small Methods*, 2021, **5**, 2001039. [17] W. Zheng, J. Yang, H. Chen, Y. Hou, Q. Wang, M. Gu, F. He, Y. Xia, Z. Xia, Z. Li, B. Yang, L. Lei, C. Yuan, Q. He, M. Qiu and X. Feng, *Adv. Fun. Mater.*, 2019, **30**, 1907658.